

Metal-Organic Framework-derived Porous Mn_{1.8}Fe_{1.2}O₄ Nanocubes with an interconnected channel structure as High-Performance Anodes for Lithium Ion Batteries

Fangcai Zheng^a, Dequan Zhu^{a#}, Xiaohui Shi and Qianwang Chen^{a,b}

^aHefei National Laboratory for Physical Science at Microscale, Department of Materials Science & Engineering & Collaborative Innovation Center of Suzhou Nano Science and Technology, University of Science and Technology of China, Hefei 230026, China.

^bHigh Magnetic Field Laboratory, Hefei Institutes of Physical Science, Chinese Academy of Sciences, Hefei 230031, China.

E-mail: cqw@ustc.edu.cn. Fax and Tel: +86 551 63603005.

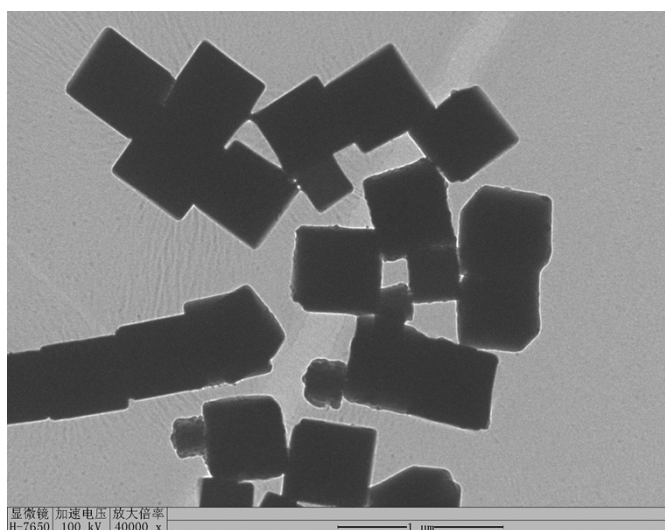


Figure S1. TEM image of Mn₃[Fe(CN)₆]₂·nH₂O nanocubes.

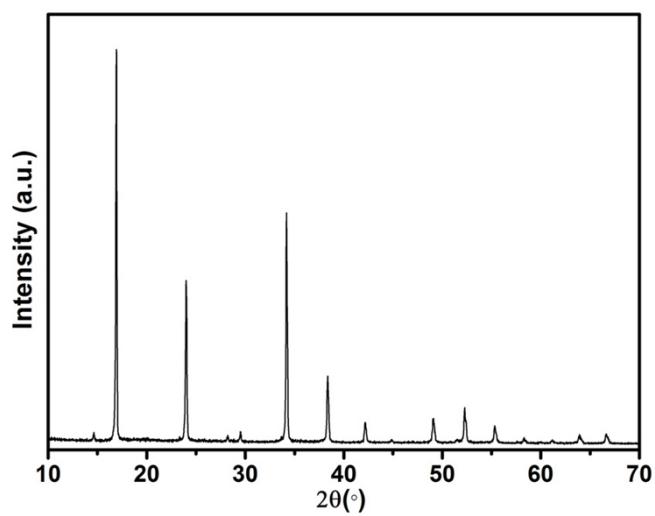


Figure S2. XRD pattern of Mn₃[Fe(CN)₆]₂·nH₂O nanocubes.

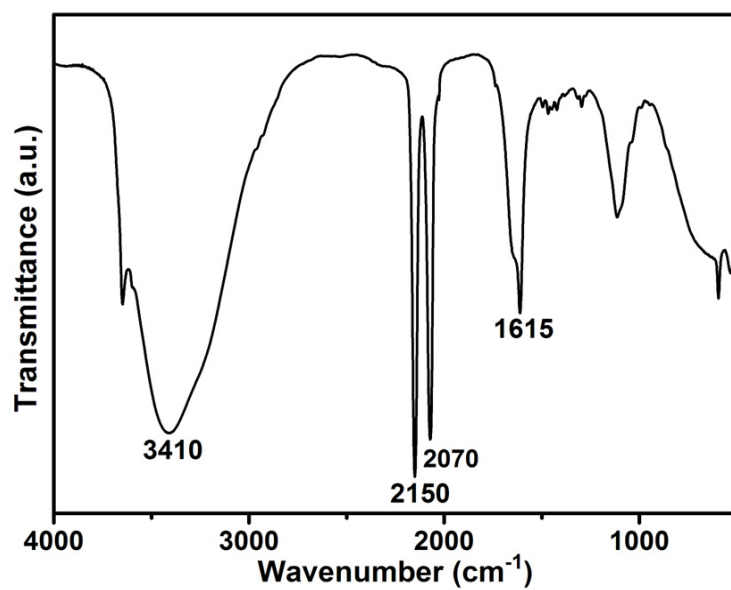


Figure S3. IR spectrum of $\text{Mn}_3[\text{Fe}(\text{CN})_6]_2 \cdot n\text{H}_2\text{O}$ nanocubes.

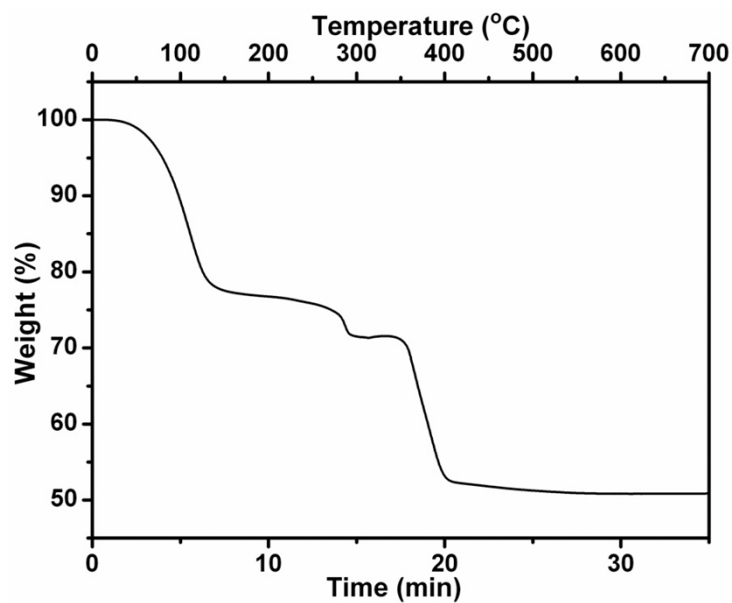


Figure S4. TGA curve of $\text{Mn}_3[\text{Fe}(\text{CN})_6]_2 \cdot n\text{H}_2\text{O}$ nanocubes under a flow of the mixed carrier gas (80 vol% He and 20 vol% O₂), with a heating rate of 20 °C min⁻¹.

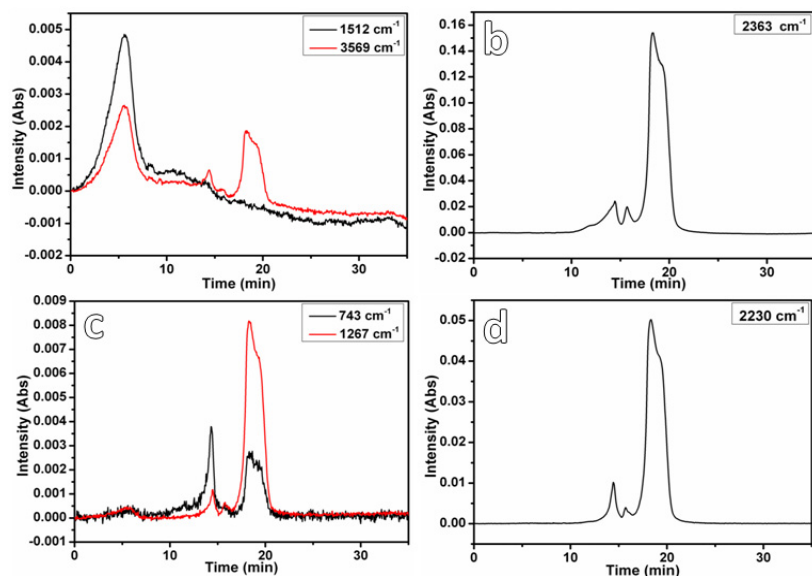


Figure S5. IR absorbance variation of (a) H₂O, (b) CO₂, (c) NO₂ and (CN)₂ as a function of time.

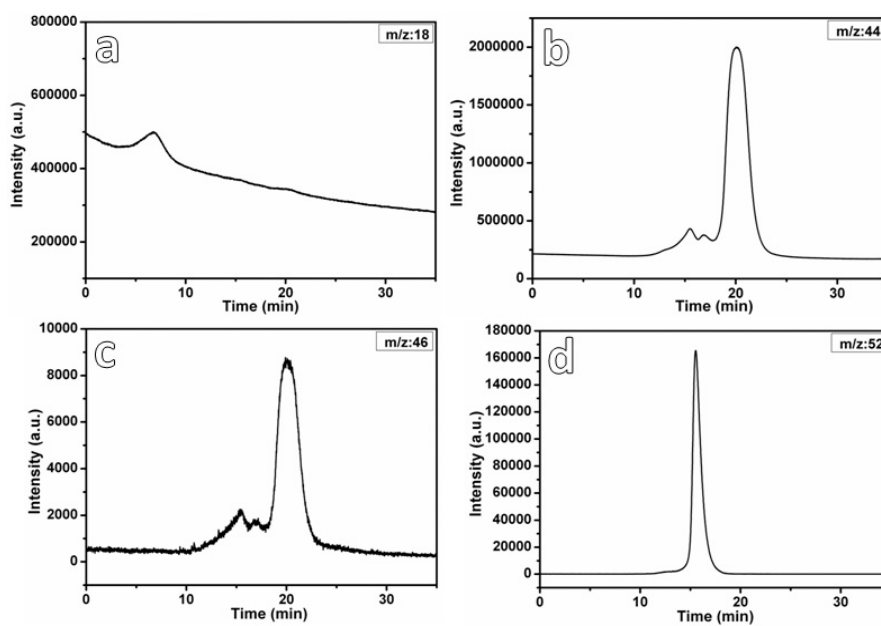


Figure S6. MS intensity variation of (a) H₂O, (b) CO₂, (c) NO₂ and (CN)₂ as a function of time.

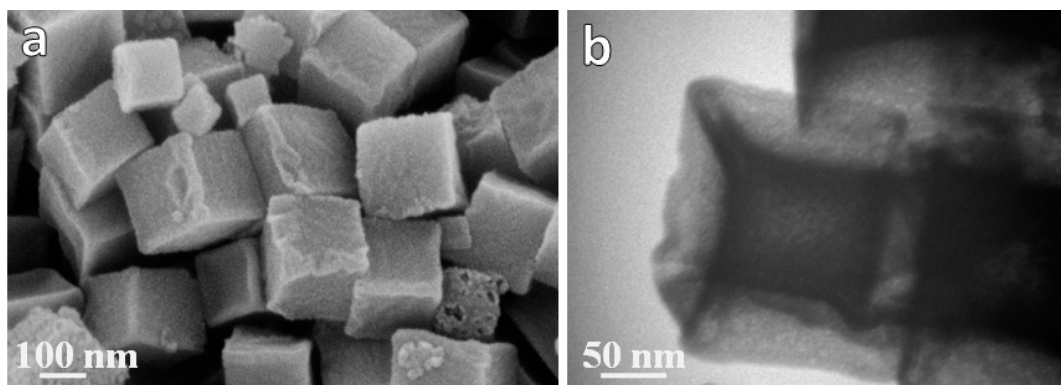


Figure S7. The high-magnification FESEM (a) and TEM (b) images of Mn_{1.8}Fe_{1.2}O₄ nanocubes.

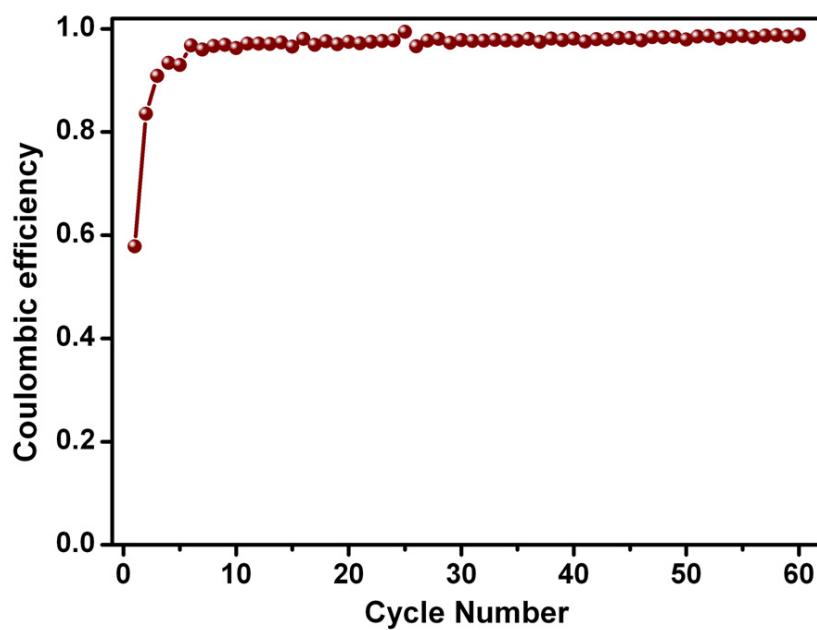


Figure S8. The coulombic efficiency of the Mn_{1.8}Fe_{1.2}O₄ nanocubes for lithium storage at a current density of 200 mA g⁻¹.

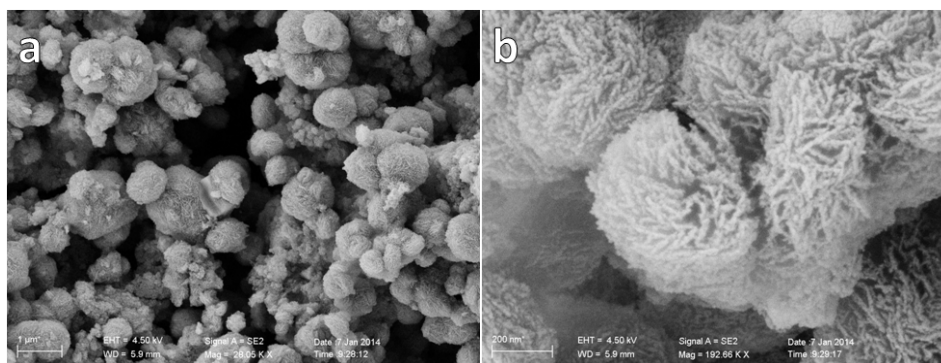


Figure S9. Morphological analysis of the electrode cycled for 20 cycles at a current density of 200 mA g^{-1} .

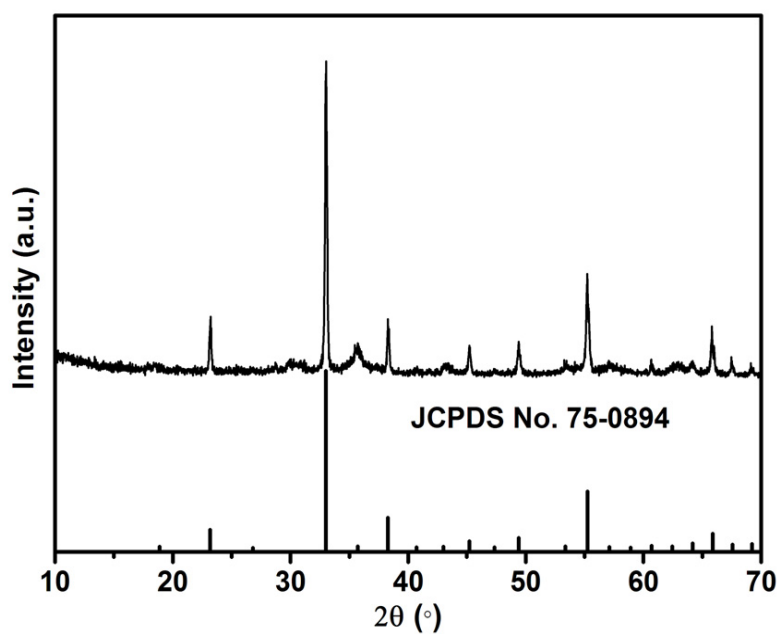


Figure S10. XRD pattern of as-prepared $\text{Mn}_x\text{Fe}_{2-x}\text{O}_3$ obtained at $600 \text{ }^\circ\text{C}$.

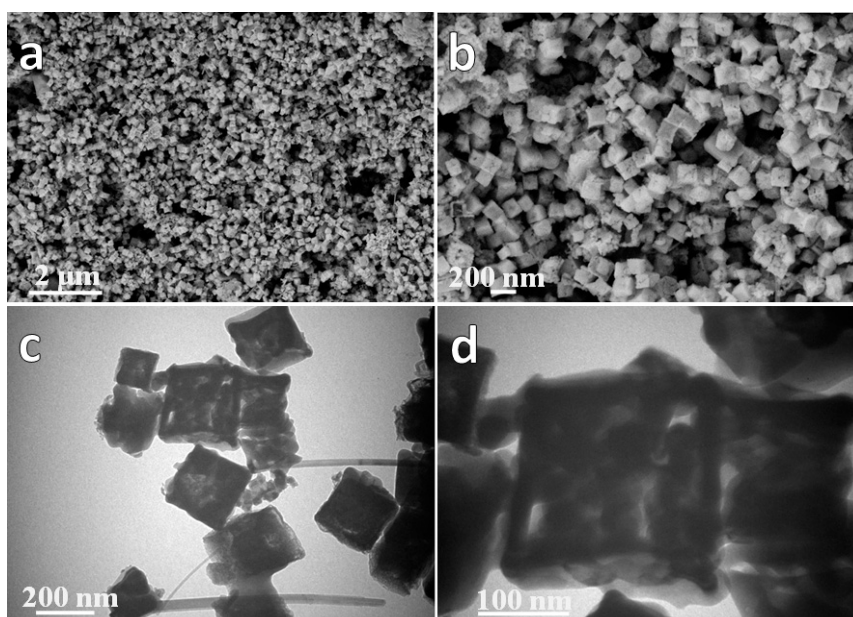


Figure S11. FESEM images of $\text{Mn}_x\text{Fe}_{2-x}\text{O}_3$ sample at different magnification (a and b). TEM images of $\text{Mn}_x\text{Fe}_{2-x}\text{O}_3$ sample at different magnification (c and d).

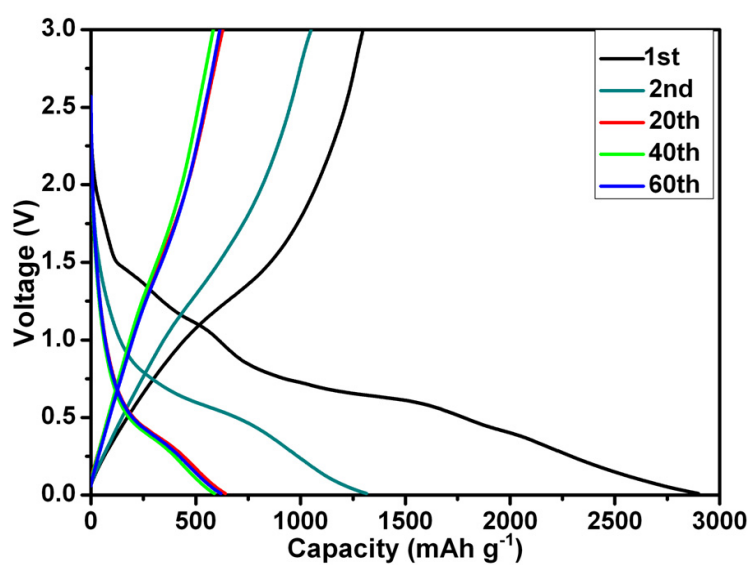


Figure S12. Discharge-charge curves of $\text{Mn}_x\text{Fe}_{2-x}\text{O}_3$ sample (600 °C) at a current density of 200 mA g^{-1} .

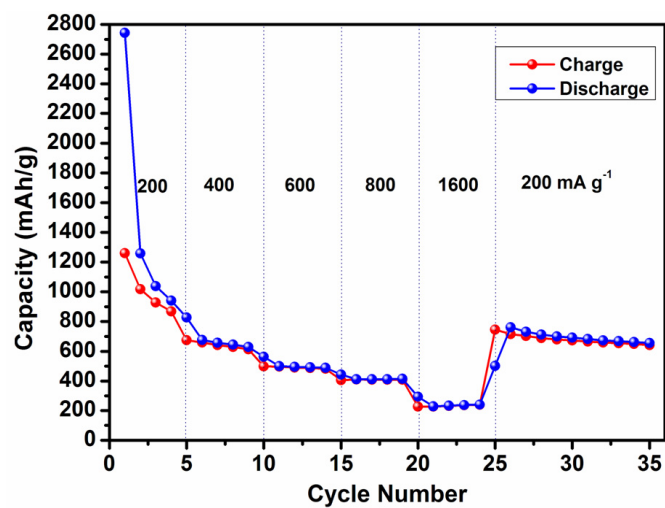


Figure S13. Rate capability test for the $\text{Mn}_x\text{Fe}_{2-x}\text{O}_3$ nanocubes at various current densities (100-1600 mA g^{-1}).